

Experimental and Computational Analysis of the Solvent-Dependent $O_2/Li^+-O_2^-$ Redox Couple: Standard Potentials, Coupling Strength, and Implications for Lithium–Oxygen Batteries

David G. Kwabi, Vyacheslav S. Bryantsev, Thomas P. Batcho, Daniil M. Itkis, Carl V. Thompson, and Yang Shao-Horn*

Abstract: Understanding and controlling the kinetics of O_2 reduction in the presence of Li^+ -containing aprotic solvents, to either $Li^+-O_2^-$ by one-electron reduction or Li_2O_2 by two-electron reduction, is instrumental to enhance the discharge voltage and capacity of aprotic $Li-O_2$ batteries. Standard potentials of $O_2/Li^+-O_2^-$ and O_2/O_2^- were experimentally measured and computed using a mixed cluster-continuum model of ion solvation. Increasing combined solvation of Li^+ and O_2^- was found to lower the coupling of $Li^+-O_2^-$ and the difference between $O_2/Li^+-O_2^-$ and O_2/O_2^- potentials. The solvation energy of Li^+ trended with donor number (DN), and varied greater than that of O_2^- ions, which correlated with acceptor number (AN), explaining a previously reported correlation between $Li^+-O_2^-$ solubility and DN. These results highlight the importance of the interplay between ion–solvent and ion–ion interactions for manipulating the energetics of intermediate species produced in aprotic metal–oxygen batteries.

Activating O_2 ^[1–4] is central to transforming energy storage by providing high gravimetric energy in devices such as rechargeable $Li-O_2$ ^[5,6] and $Na-O_2$ batteries^[7] and reversible fuel cells.^[8] Non-aqueous $Li-O_2$ batteries operate by reducing molecular O_2 in the presence of Li^+ to form Li_2O_2 at the positive electrode on discharge and releasing O_2 by oxidizing Li_2O_2 on

charge. There are, however, significant challenges to practical implementation, including poor voltage efficiency, cycle life, and power capability. These are due primarily to the lack of fundamental understanding of O_2 reduction and evolution reaction kinetics and parasitic reactions in $Li-O_2$ batteries. The kinetics of O_2 reduction in the presence of strongly coordinating Li^+ are sluggish (Supporting Information, Figure S1), and its elementary steps are not well understood. O_2 reduction proceeds first by the formation of superoxide (O_2^-)^[9,10] and then lithium superoxide ($Li^+ + O_2^- \rightarrow Li^+-O_2^-$)^[11–14]. Li_2O_2 is then formed by disproportionation of $Li^+-O_2^-$ ($2Li^+-O_2^- \rightarrow Li_2O_2 + O_2$) and/or a second electron reduction of $Li^+-O_2^-$ to solid Li_2O_2 .^[14,15] A number of studies have attributed the formation of large Li_2O_2 particles and high discharge capacities observed at low rates ($< 10 \mu A cm^{-2}$ in ethers^[16,17]), to high availability of soluble $Li^+-O_2^-$. Abraham and co-workers^[13,14,18] have suggested that the stability of $Li^+-O_2^-$ increases with solvent donor number (DN), which is a measure of the solvation enthalpy of the Lewis acid $SbCl_5$ in a given solvent.^[19] This concept is supported by recent work,^[12] which reports that increasing solvent DN leads to increased $Li^+-O_2^-$ solubility and capacities upon discharge. Understanding how standard potentials of $O_2/Li^+-O_2^-$ change in different solvents and correlating the changes with that of O_2/O_2^- and $Li^+-O_2^-$ solubility can help control the kinetics and discharge product characteristics of $Li-O_2$ batteries. Unfortunately, the standard potentials and kinetics of the $O_2/Li^+-O_2^-$ couple in aprotic solvents are not known, in contrast to extensive study of O_2 reduction to O_2^- in the presence of weakly coordinating tetrabutylammonium (TBA^+), which forms a stable $TBA^+-O_2^-$ complex^[13,14] ($TBA^+ + O_2 + e^- \leftrightarrow TBA^+-O_2^-$ in Figure 1 a; Supporting Information, Figure S1). Greater O_2^- ion solvation would be expected to stabilize $TBA^+-O_2^-$ and increase the $O_2/TBA^+-O_2^-$ redox potential,^[20] while the Li^+/Li potential decreases with increasing Li^+ solvation (Figure 1 b). These trends are consistent with reports that the reversible potential of $O_2/TBA^+-O_2^-$ increases with solvent acceptor number (AN),^[21] (a measure of solvent Lewis basicity^[22]), while that of Li^+/Li decreases with greater solvent DN.^[23] It is not straightforward, however, to estimate the $O_2/Li^+-O_2^-$ potential and its solvent dependence from AN-dependent $O_2/TBA^+-O_2^-$ and DN-dependent Li^+/Li potentials. Not only do DN and AN have different units, they also do not provide quantitative solvation energies for Li^+ and O_2^- ions. Moreover, the $O_2/Li^+-O_2^-$ potential is greatly affected by the acid–base coupling between Li^+ and O_2^- , which is not directly reflected by $O_2/TBA^+-O_2^-$ and $Li^+/$

[*] D. G. Kwabi, Prof. Y. Shao-Horn
 Department of Mechanical Engineering, Massachusetts Institute of Technology
 77 Massachusetts Avenue, Cambridge, MA 02139 (USA)
 E-mail: shaohorn@mit.edu

Dr. V. S. Bryantsev
 Liox Power Inc, 129 North Hill Ave, Suite 103, Pasadena, CA 91106 (USA)

T. P. Batcho, Prof. C. V. Thompson, Prof. Y. Shao-Horn
 Department of Materials Science and Engineering, Massachusetts Institute of Technology
 77 Massachusetts Avenue, Cambridge MA 02139 (USA)

Dr. D. M. Itkis
 Department of Chemistry and Materials Science, Moscow State University
 Moscow, 119992 (Russia)

Dr. V. S. Bryantsev
 Current address: Oak Ridge National Lab, Chemical Sciences Division
 1 Bethel Valley Rd, Oak Ridge, TN 37831-6119 (USA)

Supporting information for this article is available on the WWW under <http://dx.doi.org/10.1002/anie.201509143>.

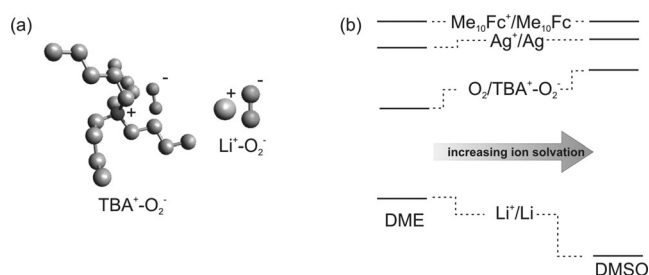


Figure 1. a) $\text{TBA}^+\text{-O}_2^-$ and $\text{Li}^+\text{-O}_2^-$ complexes and b) the effect of increasing O_2^- and Li^+ ion solvation from weakly to strongly solvating media (such as DME to DMSO) on $\text{O}_2/\text{TBA}^+\text{-O}_2^-$ and Li^+/Li redox potentials measured using an Ag/Ag^+ reference electrode and $\text{Me}_{10}\text{Fc}^+/\text{Me}_{10}\text{Fc}$ as a solvent independent redox reference.

Li potentials, and cannot be inferred from hard-soft acid-base theory.^[24]

Herein we report for the first time increasing standard $\text{O}_2/\text{TBA}^+\text{-O}_2^-$ potentials with greater AN and decreasing Li^+/Li redox potentials with DN for a series of aprotic solvents, referenced to the solvent-independent decamethylferrocenium/decamethylferrocene ($\text{Me}_{10}\text{Fc}^+/\text{Me}_{10}\text{Fc}$) redox couple, which is stable against O_2^- , unlike ferrocenium (Fc^+) in the Fc^+/Fc couple.^[25] The measured redox potentials of $\text{O}_2/\text{TBA}^+\text{-O}_2^-$ and Li^+/Li are in agreement with standard potentials computed using a mixed cluster-continuum model, which increase and decrease with greater computed solvation energy of O_2^- and Li^+ , respectively. Of significance, we show that greater Li^+ and O_2^- solvation correlates with weakened coupling strength of $\text{Li}^+\text{-O}_2^-$, as evidenced by decreasing differences between measured $\text{O}_2/\text{Li}^+\text{-O}_2^-$ and $\text{O}_2/\text{TBA}^+\text{-O}_2^-$ standard potentials.

We first show that measured standard potentials of $\text{O}_2/\text{TBA}^+\text{-O}_2^-$ and Li^+/Li scale with computed solvation energy of O_2^- and Li^+ . The use of higher AN solvents led to higher $\text{O}_2/\text{TBA}^+\text{-O}_2^-$ redox potentials, as indicated in Figure 1 b and previous work.^[20,21]

Figure 2 a shows cyclic voltammograms (CVs) obtained in O_2 -saturated dimethylsulfoxide (DMSO), 1,2-dimethoxyethane (DME), acetonitrile (MeCN), and dimethyl acetamide (DMA)-based electrolytes, which contained TBA^+ and Me_{10}Fc . Similar measurements were performed in dimethyl formamide (DMF; Supporting Information, Figure S2). These media were chosen because they are kinetically stable against superoxide^[20,26,27] and have been proposed as candidate electrolyte solvents for Li-O_2 batteries.^[28-30] Standard $\text{O}_2/\text{TBA}^+\text{-O}_2^-$ redox potentials referenced to $\text{Me}_{10}\text{Fc}^+/\text{Me}_{10}\text{Fc}$ were found to increase linearly ($R^2=0.98$) with greater AN, where the largest difference of about 0.2 V was noted between DME and DMSO (Figure 2b; Supporting Information, Figure S3). Such an excellent linear correlation between solvent AN and $\text{O}_2/\text{TBA}^+\text{-O}_2^-$ redox potential makes it unlikely that changes in $\text{O}_2/\text{TBA}^+\text{-O}_2^-$ redox energetics are determined by other species, or minor impurities such as water. This correlation is also in agreement with a previous correlation between AN and $\text{O}_2/\text{TBA}^+\text{-O}_2^-$ vs. Fc^+/Fc (Supporting Information, Figure S4a, $R^2=0.99$).^[21] The correlations established using these solvent-independent

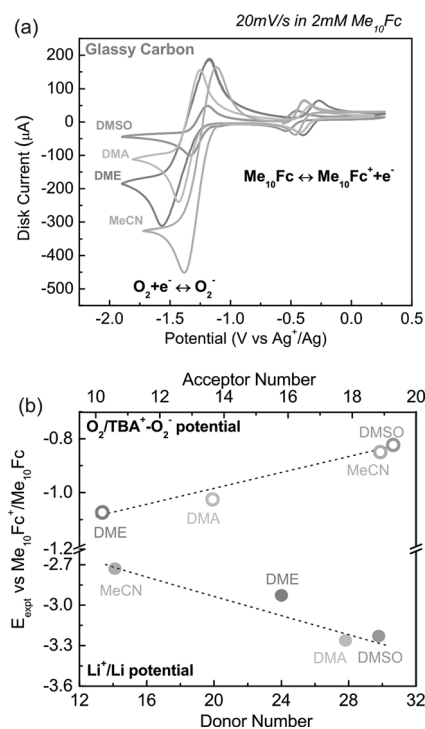


Figure 2. a) Steady-state CVs of $\text{O}_2/\text{TBA}^+\text{-O}_2^-$ and $\text{Me}_{10}\text{Fc}^+/\text{Me}_{10}\text{Fc}$ redox reactions collected at 20 mV s^{-1} in O_2 -saturated electrolytes containing $2\text{ mM Me}_{10}\text{Fc}$ in 0.5 M TBAClO_4 in DME, 0.1 M TBAClO_4 in DMA, and DMSO, obtained with an Ag/Ag^+ reference electrode and Ni foam counter electrode. b) Experimental standard $\text{O}_2/\text{TBA}^+\text{-O}_2^-$ and Li^+/Li redox potentials vs. $\text{Me}_{10}\text{Fc}^+/\text{Me}_{10}\text{Fc}$ plotted against acceptor and donor numbers of each solvent.

references are much improved in comparison to the trend obtained using the solvent-dependent Ag/Ag^+ reference reported by Sawyer et al.^[20] (Supporting Information, Figure S4b, $R^2=0.75$).

Li^+/Li redox potentials were found to decrease with greater DN (Figure 2b) in accordance with the trend suggested in Figure 1b, and had values vs. $\text{Me}_{10}\text{Fc}^+/\text{Me}_{10}\text{Fc}$ consistent with other ferrocene derivatives.^[31] Li^+/Li potentials were obtained from Li plating/stripping CV measurements vs. Ag^+/Ag , which were then referenced to the $\text{Me}_{10}\text{Fc}^+/\text{Me}_{10}\text{Fc}$ potential using the scaling found between $\text{Me}_{10}\text{Fc}^+/\text{Me}_{10}\text{Fc}$ and Ag^+/Ag . The CVs in 0.1 M LiClO_4 in DMSO, DME, MeCN and DMA are shown in the Supporting Information, Figure S5a. The redox potential of Li^+/Li ($\text{Li}^+ + \text{e}^- \leftrightarrow \text{Li}$) was defined from the potential at zero current (that is, where neither Li plating nor removal occurs) during the anodic scan. Decreasing Li^+/Li redox potentials with greater DN obtained from this method is in accordance with the trend obtained using open-circuit voltage measurements (Supporting Information, Figure S5b and Table S1). Reported higher Li-O_2 discharge potentials in DMSO than in ether-based solvents such as tetraglyme (200 mV)^[32] and DME (ca. 250 mV)^[33] can be attributed largely to lower Li^+/Li redox in DMSO by 300 mV than DME (Figure 2b). Further evidence for increasing $\text{O}_2/\text{TBA}^+\text{-O}_2^-$ and decreasing Li^+/Li redox potentials with greater solvation came from single-ion O_2^- and Li^+ solvation energy calculations in DMSO, DME,

MeCN and DMA (Figure 3) using a mixed cluster-continuum model. These solvation free energies O_2^- and Li^+ were referenced to the ion free energy in the gas phase and computed according to Figure 3a. The most stable ion-solvent clusters for O_2^- in DMSO and DME are shown in Figure 3b as examples, from which single-ion solvation free energies were obtained (Supporting Information, Table S2). The computed solvation free energy, $\Delta G_{solv}^*(O_2^-)$, was found to increase with greater AN ($R^2 = 0.81$), from -259 kJ mol^{-1} in DME to -315 kJ mol^{-1} in DMSO, as shown in the Supporting Information, Table S2. The absolute O_2 reduction potential (O_2/O_2^-) was computed with respect to electron energy in a vacuum, using:

$$-FE_{(abs)}^* = \Delta_f G_{298}^0[O_2^-(g)] + \Delta G^{o-*} + \Delta G_{solv}^*[O_2^-(g)] \quad (1)$$

where $\Delta_f G_{298}^0[O_2^-(g)]$ and ΔG^{o-*} are solvent-independent parameters related to gas-phase ionization and standard state correction, respectively (see details in Supporting information). Computed O_2/O_2^- redox potentials referenced to DME show a good agreement with, but are consistently higher than measured $O_2/TBA^+-O_2^-$, as shown in Figure 3c. This could originate from a combination of computational inaccuracy and computed O_2/O_2^- potentials not accounting for $TBA^+-O_2^-$ pairing which, although weak, would partially neutralize and therefore reduce the effective solvation of O_2^- in experimental measurements.

The computed solvation free energy, $\Delta G_{solv}^*(Li^+)$, was found to linearly increase with greater DN ($R^2 > 0.99$), from

-509 kJ mol^{-1} in MeCN to -557 kJ mol^{-1} in DMSO, as shown in Figure 3c. On the other hand, $\Delta G_{solv}^*(Li^+)$ did not scale with AN ($R^2 = 0.02$) (Supporting Information, Figure S6). The absolute potential of Li^+/Li decreased linearly with lower $\Delta G_{solv}^*(Li^+)$, which was computed using:

$$-FE_{(abs)}^* = \Delta_f G_{298}^0[Li^+(g)] + \Delta G^{o-*} + \Delta G_{solv}^*[Li^+(g)] \quad (2)$$

with $\Delta_f G_{298}^0[Li^+(g)]$ and ΔG^{o-*} being solvent-independent variables related to gas-phase ionization (including the Li sublimation energy) and standard state correction, respectively.

Remarkably, computed solvent-dependent changes in the Li^+/Li redox potential referenced to MeCN showed an excellent agreement compared with measured differences, as shown in Figure 3c. The most stable Li^+ -solvent clusters with cluster size $n = 4$ for DMSO and 3 for DME are shown in Figure 3b, from which single ion solvation free energies were obtained (Supporting Information, Table S3). As greater Li^+ solvation lowers the Li^+/Li potential while greater O_2^- solvation increases the O_2/O_2^- potential, solvents that strongly solvate both Li^+ and O_2^- have high O_2/O_2^- potentials vs. Li^+/Li potentials. Indeed, the $O_2/TBA^+-O_2^-$ redox potentials referenced to the Li^+/Li scale increased with greater combined solvation of O_2^- and Li^+ (Figure 3d), and were in close agreement with computed standard O_2 reduction potential of O_2/O_2^- vs. Li^+/Li (Supporting Information, Tables S4–S5), and previous experimental findings reporting higher $O_2/TBA^+-O_2^-$ redox potentials vs. Li^+/Li of 2.25^[34] and 2.37^[14] V in DMSO, compared to about 2.0 V for DME, MeCN,^[14] and ionic liquids.^[35]

Solvent-dependent $O_2/Li^+-O_2^-$ redox potentials in Li^+ -containing DMSO, DME, DMA, and DMF were estimated using chronoamperometric rotating ring-disk electrode (RRDE) measurements. The disk was held at a potential to reduce O_2 under rotation at 900 rpm while the ring was held at discrete potentials to oxidize soluble intermediate species that diffused from the disk (Supporting Information, Figure S7). Ring current transients measured from 3.50 to 2.76 V vs. Li^+/Li (Figure 4a) with the disk potential kept at 2.6 V vs. Li^+/Li (Figure 4b) in DMSO are shown as an example (for those for other solvents, see the Supporting Information, Figure S8). Ring currents were found to decrease with reducing potentials from 3.7 V to 2.7 V vs. Li^+/Li for all solvents examined, which can be attributed to the ring potential approaching the equilibrium potential for soluble intermediate oxidation. We hypothesize that soluble ORR intermediates oxidized on the ring are $Li^+-O_2^-$ -like species. This is supported by previous in situ electrochemical quartz microbalance^[36]

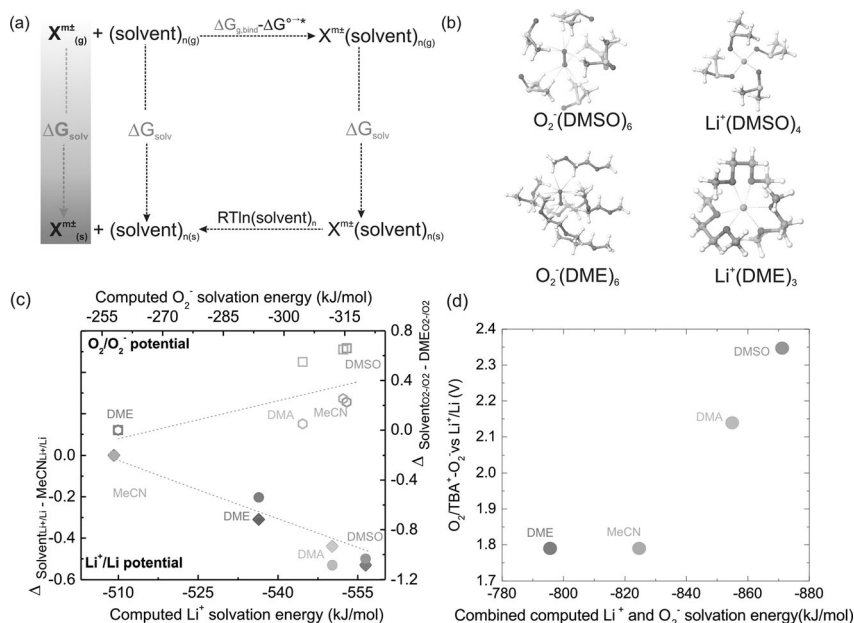


Figure 3. a) Thermodynamic cycle for the calculation of Li^+ or O_2^- ion solvation. b) Structures of the most stable $X(solvent)_n$ clusters (solvent = DMSO, DME; $X = Li^+, O_2^-$, $n = 3-6$) obtained at the M06-L/6-311++G**//B3LYP/6-31G** level. c) Comparison of standard experimental (open hexagons) and calculated (open squares) O_2/O_2^- and experimental (filled circles) and calculated (filled diamonds) Li^+/Li redox potentials against computed Li^+ and O_2^- solvation energies of each solvent. All Li^+/Li and O_2/O_2^- potentials are plotted with respect to MeCN and DME, respectively. d) Standard experimental redox potentials of $O_2/TBA^+-O_2^-$ vs. Li^+/Li against combined Li^+ and O_2^- solvation energy.

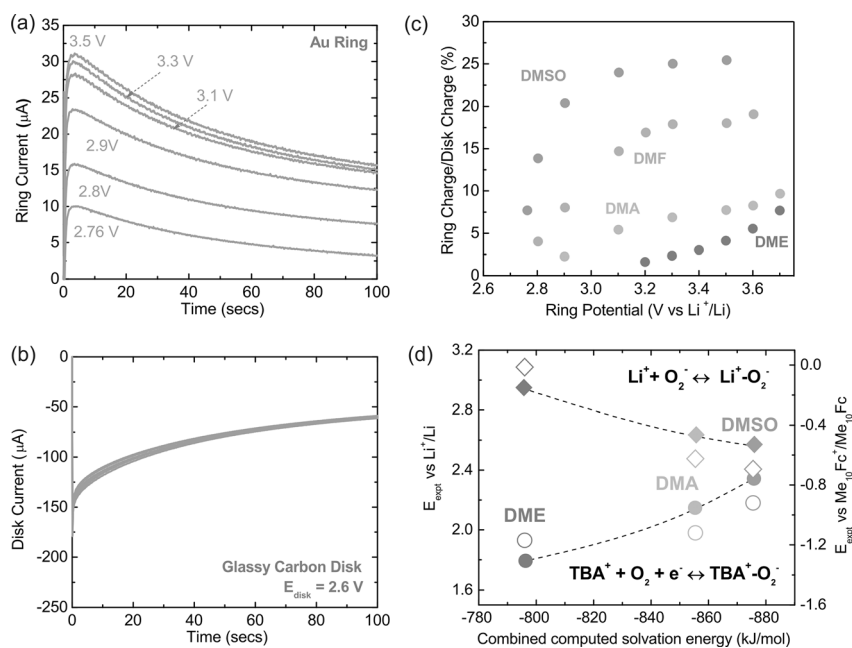


Figure 4. a) Ring current transients during RRDE measurements in 0.1 M LiClO₄ in DMSO at 900 rpm with disk held at 2.6 V vs. Li⁺/Li b) Disk current transients during RRDE measurements in 0.1 M LiClO₄ in DMSO at 900 rpm with disk held at 2.6 V vs. Li⁺/Li c) Variation of ring-to-disk charge ratios for potentiostatic experiments in 0.1 M LiClO₄ in DMSO, DME, DMA, and DMF at ring potentials between 2.75 and 3.70 V vs. Li⁺/Li. The RRDE was rotated at 900 rpm for all measurements d) Relationship between standard redox potentials for O₂/TBA⁺-O₂⁻ (circles) and O₂/Li⁺-O₂⁻ (diamonds) vs. Li⁺/Li (filled symbols) and Me₁₀Fc⁺/Me₁₀Fc (open symbols) and the total solvation energy for Li⁺ and O₂⁻ ions calculated from a mixed cluster-continuum model for each solvent.

(EQCM) analysis and surface-enhanced Raman scattering (SERS)^[11,12] studies. Of significance to note is that the appearance of a peak at 1137 cm⁻¹ in the SERS^[11,12] studies has been assigned to the formation of Li⁺-O₂⁻ due to its slightly higher wavenumber than TBA⁺-O₂⁻, which is consistent with a strengthening of the O—O⁻ bond due to Li⁺-O₂⁻ coupling. We caution that the molecular structure of the Li⁺-O₂⁻-like intermediate is not completely understood, that is, whether it exists in solvent-separated or contact ion pairs, or (Li⁺-O₂⁻)_n-type aggregates.^[12,37] Thus, the redox potentials for O₂/Li⁺-O₂⁻ measured from RRDE may reflect the energetics of Li⁺-O₂⁻-related clusters,^[37] or Li⁺-O₂⁻ species adsorbed to the Au ring surface rather than soluble, “molecular” Li⁺-O₂⁻-like species. Standard O₂/Li⁺-O₂⁻ potentials extrapolated from chronoamperometric measurements of the ring/disk charge ratio are shown in Figure 4c, and reveal increasing O₂/Li⁺-O₂⁻ potentials from DMSO, DMA, DMF, to DME. O₂/Li⁺-O₂⁻ potentials in MeCN could not be measured owing to very low ring currents, which fall within experimental uncertainty as a result of negligible solubility of Li⁺-O₂⁻ in MeCN (Supporting Information, Figure S9e), in agreement with previous RRDE studies.^[12,33,38] Standard potentials were obtained by correcting extrapolated values in Figure 4d for O₂ solubility and Li⁺ concentration (see the Supporting Information). Of significance to note is that standard O₂/Li⁺-O₂⁻ redox potentials referenced to both Li⁺/Li and solvent-independent Me₁₀Fc⁺/Me₁₀Fc (Figure 4d) decrease considerably with increasing combined solvation energy computed for

Li⁺ and O₂⁻ ions on the absolute energy scale, while standard O₂/TBA⁺-O₂⁻ potentials increased with increasing computed combined solvation of O₂⁻ and Li⁺ (Figure 4d). This resulted in a reduction in the difference between standard O₂/TBA⁺-O₂⁻ and O₂/Li⁺-O₂⁻ potentials with increasing combined solvation, which is in agreement with the trend in computed O₂/Li⁺-O₂⁻ and O₂/O₂⁻ redox potentials found in DMSO, DME, MeCN and DMA (Supporting Information, Table S6 and Figure S10a). We note that although experimental standard O₂/Li⁺-O₂⁻ redox potentials would be expected to increase with combined solvation energy of Li⁺ and O₂⁻, they were found to decrease in this study. This observation can be attributed to additional contributions to the energetics of Li⁺-O₂⁻ formation beyond solvation, such as the formation of Li⁺-O₂⁻ aggregates or Li⁺-O₂⁻ species adsorbed to the Au ring, as noted above.

The reduction in the difference between standard O₂/TBA⁺-O₂⁻ and O₂/Li⁺-O₂⁻ potentials with increasing combined solvation can be attributed to increasing solvation of Li⁺ and O₂⁻, which reduces coupling of solvated Li⁺ to O₂⁻, as shown in Figure 4d and the Supporting Information, Table S7. The coupling energy of Li⁺-O₂⁻ relative to TBA⁺-O₂⁻, described as the Gibbs free energy of Li⁺ + TBA⁺-O₂⁻ → Li⁺-O₂⁻ + TBA⁺, can be estimated from the difference between standard potentials of O₂/Li⁺-O₂⁻ and previously obtained O₂/TBA⁺-O₂⁻ measurements (Supporting Information, Table S7). Interestingly, the Li⁺-O₂⁻ coupling energy gain decreased with increasing combined computed solvation energy of Li⁺ and O₂⁻ ions, as shown in Figure 5a and the Supporting Information, Table S6. For example, the difference between standard O₂/Li⁺-O₂⁻ and O₂/TBA⁺-O₂⁻ redox potentials in DME is 1.24 V, yielding Li⁺-O₂⁻ coupling of -120 kJ mol⁻¹. In contrast, smaller Li⁺-O₂⁻ coupling energies of -21 kJ mol⁻¹ in DMSO and -47 kJ mol⁻¹ in DMA were found (Supporting Information, Table S7 and Figure S10b). Li⁺-O₂⁻ coupling energies obtained from experimental O₂/TBA⁺-O₂⁻ and O₂/Li⁺-O₂⁻ redox potentials in this study are considerably more negative than those from previous work based on thermochemical data of solid Li⁺-O₂⁻^[12] which does not take into consideration Li⁺-O₂⁻ solvation, resulting in weak coupling in DME (-25 kJ mol⁻¹) and thermodynamically unfavorable coupling for DMSO (20 kJ mol⁻¹). Thermodynamically favorable coupling for Li⁺-O₂⁻ is supported by observations that Li₂O₂ readily forms upon the addition of a Li⁺ salt to superoxide (KO₂)-containing suspensions of DME and DMSO.^[39–41]

We find that increasing O₂⁻ and Li⁺ solvation, as expressed by O₂/TBA⁺-O₂⁻ redox potentials vs. Li⁺/Li, increases the solubility of Li⁺-O₂⁻ in the solvent, as shown

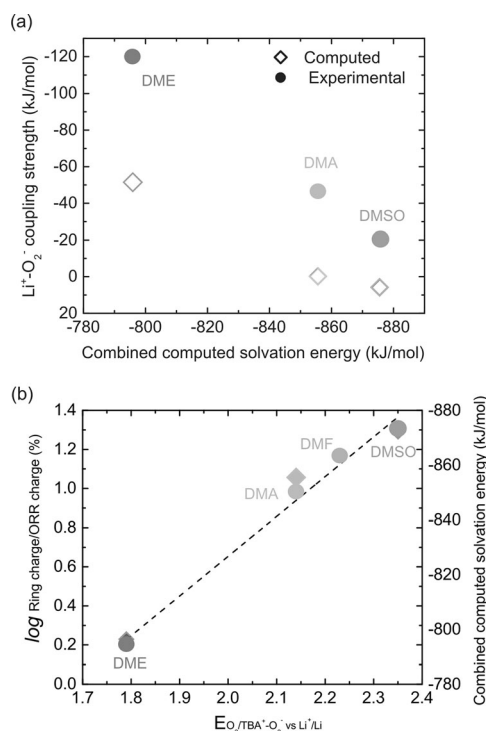


Figure 5. Comparison between a) combined computed solvation energy of Li⁺ and O₂⁻ ions in DMSO, DME, and DMA and computed (diamonds) and experimental (circles) Li⁺-O₂⁻ coupling energies and b) O₂/TBA⁺-O₂⁻ vs. Li⁺/Li redox potentials with the logarithm of ring-to-disk charge during Li-ORR (circles) and combined computed solvation energy of Li⁺ and O₂⁻ ions in DMSO, DME, DMA, and DMF (diamonds). Dotted line shows linear regression through experimental data, R² = 0.98.

in Figure 5b. Li⁺-O₂⁻ solubility was assessed using the logarithm of the ring-to-disk charge ratio obtained during ORR from RRDE measurements with the ring kept at 3.5 V vs. Li⁺/Li (Supporting Information, Figures S9 and S11). Li⁺-O₂⁻ solubility was found to increase linearly (DME < DMA < DMF < DMSO) with combined computed solvation energies of Li⁺ and O₂⁻, and measured (Figure 5b) and computed (Supporting Information, Figure S12a) O₂/TBA⁺-O₂⁻ redox potentials vs. Li⁺/Li.

A previously reported correlation between Li⁺-O₂⁻ solubility and DN^[12] (Supporting Information, Figure S12b) can be attributed to the fact that the combined computed solvation energy is dominated by computed Li⁺ solvation energies (which scales with DN), as computed Li⁺ solvation energies are considerably higher than those of O₂⁻. However, considering Li⁺ solvation (or DN) alone cannot explain trends in the Li⁺-O₂⁻ solubility for solvents with similar DN's but different AN's such as DMF (DN = 26.6 and AN = 16.0) and DMA (DN = 27.8 and 13.6), where greater Li⁺-O₂⁻ solubility observed for DMF than DMA cannot be explained by DN (Supporting Information, Figure S12c). Extending this understanding to non-aqueous Na-O₂ and K-O₂ electrochemistry, it would be expected that the solubility of Na⁺-O₂⁻ and K⁺-O₂⁻ would not scale with DN as well, as Na⁺ and K⁺ are weaker Lewis acids than Li⁺ and will be solvated less strongly. This is supported by a recent computational study of de-solvation

energies of Li⁺ and Na⁺ in 27 organic solvents,^[42] which found that Na⁺ de-solvation energies were on average 20% less than Li⁺, implying weaker Na⁺ solvation in non-aqueous solvents. Similarly, computed gas-phase binding energies of Na⁺ and K⁺ to tetrahydrofuran have been reported to be much less than that for Li⁺,^[43] and comparable to the computed solvation energies of O₂⁻, $\Delta G_{\text{solv}}^*(\text{O}_2^-)$, as found in this study.

Understanding and controlling the solvation and coupling of O₂⁻ and Li⁺ ions has far-reaching implications for developing reversible Li-O₂ battery electrochemistry. Increasing Li⁺-O₂⁻ solubility can suppress surface nucleation rates^[44] or trigger solution-phase growth of Li₂O₂,^[12,16] resulting in high discharge capacities by increased pore filling with large, solid Li₂O₂ agglomerates.^[17,45,46] However, solvents with high Li⁺-O₂⁻ solubilities such as DMSO can be more subject to superoxide attack and decrease solvent stability in Li-O₂ batteries.^[47-49] This argument is supported by increasing computed $\Delta G_{\text{solv}}^*(\text{O}_2^-)$ with decreasing computed pK_a of solvents (in DMSO; Supporting Information, Table S2), and previous findings which established a correlation between solvent AN and DN, and pK_a, where solvents with higher Li⁺-O₂⁻ solubility were more susceptible to proton abstraction by O₂⁻.^[50] As Li⁺ solvation structures can vary greatly among similar solvents (for example, glymes),^[51,52] and across different classes of solvents such as ionic liquids,^[53] caution should be exercised and further studies are needed to examine the influence of solvation and coupling of O₂⁻ and Li⁺ ions on solvent stability.

In summary, we have shown that standard potentials of the O₂/Li⁺-O₂⁻ redox reaction becomes comparable to those of O₂/TBA⁺-O₂⁻ with increasing combined solvation energy of Li⁺ and O₂⁻ ions, owing to reduced coupling energy of Li⁺-O₂⁻. Furthermore, we have shown that Li⁺-O₂⁻ solubility increases with greater combined solvation energy of O₂⁻ and Li⁺, which can be correlated with experimental standard O₂/TBA⁺-O₂⁻ potentials. These results highlight the importance of the interplay between ion-solvent and ion-ion interactions in understanding and controlling the intermediate species energetics, reaction product morphology, discharge capacity, and solvent stability in aprotic metal-O₂ batteries.

Acknowledgements

This work was supported in part by the MRSEC Program of the National Science Foundation under award number DMR-0819762, the Robert Bosch Company with a Bosch Energy Research Network Grant, the CERC-CVC (China Clean Energy Research Center-Clean Vehicles Consortium) US of the Department of Energy (under award number DE-PI0000012), and the Skoltech-MIT Center for Electrochemical Energy Storage. SEM imaging was performed at the Center for Nanoscale Systems (CNS), a member of the National Nanotechnology Infrastructure Network, which is supported by the National Science Foundation under NSF award no. ECS-0335765. CNS is part of Harvard University.

Keywords: acid-base interactions · lithium · oxygen electrochemistry · solvation · superoxide

- [1] N. S. Lewis, D. G. Nocera, *Proc. Natl. Acad. Sci. USA* **2007**, *104*, 20142.
- [2] H. B. Gray, *Nat. Chem.* **2009**, *1*, 7.
- [3] H. A. Gasteiger, N. M. Marković, *Science* **2009**, *324*, 48–49.
- [4] G. M. Whitesides, G. W. Crabtree, *Science* **2007**, *315*, 796–798.
- [5] P. G. Bruce, S. A. Freunberger, L. J. Hardwick, J.-M. Tarascon, *Nat. Mater.* **2012**, *11*, 19–29.
- [6] D. G. Kwabi, N. Ortiz-Vitoriano, S. A. Freunberger, Y. Chen, N. Imanishi, P. G. Bruce, Y. Shao-Horn, *MRS Bull.* **2014**, *39*, 443–452.
- [7] P. Hartmann, C. L. Bender, M. Vračar, A. K. Dürr, A. Garsuch, J. Janek, P. Adelhelm, *Nat. Mater.* **2012**, DOI: 10.1038/nmat3486.
- [8] R. F. Service, *Science* **2009**, *324*, 1257–1259.
- [9] D. T. Sawyer, M. J. Gibian, *Tetrahedron* **1979**, *35*, 1471–1481.
- [10] D. L. Maricle, W. G. Hodgson, *Anal. Chem.* **1965**, *37*, 1562–1565.
- [11] Z. Peng, S. A. Freunberger, L. J. Hardwick, Y. Chen, V. Giordani, F. Bardé, P. Novák, D. Graham, J.-M. Tarascon, P. G. Bruce, *Angew. Chem. Int. Ed.* **2011**, *50*, 6351–6355; *Angew. Chem.* **2011**, *123*, 6475–6479.
- [12] L. Johnson, C. Li, Z. Liu, Y. Chen, S. A. Freunberger, J.-M. Tarascon, P. C. Ashok, B. B. Praveen, K. Dholakia, P. G. Bruce, *Nat. Chem.* **2014**, *6*, 1091–1099.
- [13] C. O. Laoire, S. Mukerjee, K. M. Abraham, E. J. Plichta, M. A. Hendrickson, *J. Phys. Chem. C* **2009**, *113*, 20127–20134.
- [14] C. O. Laoire, S. Mukerjee, K. M. Abraham, E. J. Plichta, M. A. Hendrickson, *J. Phys. Chem. C* **2010**, *114*, 9178–9186.
- [15] B. D. McCloskey, R. Scheffler, A. Speidel, G. Girishkumar, A. C. Luntz, *J. Phys. Chem. C* **2012**, *116*, 23897–23905.
- [16] L. Nazar, B. Adams, R. Black, C. Radtke, K. Zaghib, M. Trudeau, *Energy Environ. Sci.* **2013**, DOI: 10.1039/c3ee40697k.
- [17] B. M. Gallant, D. G. Kwabi, R. R. Mitchell, J. Zhou, C. Thompson, Y. Shao-Horn, *Energy Environ. Sci.* **2013**, *6*, 2518–2528.
- [18] K. M. Abraham, *J. Electrochem. Soc.* **2015**, *162*, A3021–A3031.
- [19] V. Gutmann, *Coord. Chem. Rev.* **1976**, *18*, 225–255.
- [20] D. T. Sawyer, G. Chiericato, C. T. Angells, E. J. Nanni, T. Tsuchiya, *Anal. Chem.* **1982**, *54*, 1720–1724.
- [21] V. S. Bryantsev, V. Giordani, W. Walker, M. Blanco, S. Zecevic, K. Sasaki, J. Uddin, D. Addison, G. V. Chase, *J. Phys. Chem. A* **2011**, *115*, 12399–12409.
- [22] U. Mayer, V. Gutmann, W. Gerger, *Monatsh. Chem.* **1975**, *106*, 1235–1257.
- [23] G. Grützner, *J. Phys. Chem.* **1986**, *90*, 5478–5485.
- [24] R. G. Pearson, *J. Am. Chem. Soc.* **1963**, *85*, 3533–3539.
- [25] I. Noviantri, K. N. Brown, D. S. Fleming, P. T. Gulyas, P. A. Lay, A. F. Masters, L. Phillips, *J. Phys. Chem. B* **1999**, *103*, 6713–6722.
- [26] D. Aurbach, M. Daroux, P. Faguy, E. Yeager, *J. Electroanal. Chem. Interfacial Electrochem.* **1991**, *297*, 225–244.
- [27] V. S. Bryantsev, J. Uddin, V. Giordani, W. Walker, D. Addison, G. V. Chase, *J. Electrochem. Soc.* **2012**, *160*, A160–A171.
- [28] S. A. Freunberger, Y. Chen, N. E. Drewett, L. J. Hardwick, F. Bardé, P. G. Bruce, *Angew. Chem. Int. Ed.* **2011**, *50*, 8609–8613; *Angew. Chem.* **2011**, *123*, 8768–8772.
- [29] Y. Chen, S. A. Freunberger, Z. Peng, F. Barde, P. G. Bruce, *J. Am. Chem. Soc.* **2012**, *134*, 7952–7957.
- [30] W. Walker, V. Giordani, J. Uddin, V. S. Bryantsev, G. V. Chase, D. Addison, *J. Am. Chem. Soc.* **2013**, *135*, 2076–2079.
- [31] M. N. Ates, C. J. Allen, S. Mukerjee, K. M. Abraham, *J. Electrochem. Soc.* **2012**, *159*, A1057–A1064.
- [32] D. Xu, Z. Wang, J. Xu, L. Zhang, X. Zhang, *Chem. Commun.* **2012**, *48*, 6948–6950.
- [33] M. J. Trahan, S. Mukerjee, E. J. Plichta, M. A. Hendrickson, K. M. Abraham, *J. Electrochem. Soc.* **2013**, *160*, A259–A267.
- [34] Y. Chen, S. A. Freunberger, Z. Peng, O. Fontaine, P. G. Bruce, *Nat. Chem.* **2013**, *5*, 489–494.
- [35] C. J. Allen, J. Hwang, R. Kautz, S. Mukerjee, E. J. Plichta, M. A. Hendrickson, K. M. Abraham, *J. Phys. Chem. C* **2012**, *116*, 20755–20764.
- [36] D. Sharon, V. Etacheri, A. Garsuch, M. Afri, A. A. Frimer, D. Aurbach, *J. Phys. Chem. Lett.* **2012**, *3*, 127–131.
- [37] U. Das, K. C. Lau, P. C. Redfern, L. A. Curtiss, *J. Phys. Chem. Lett.* **2014**, *5*, 813–819.
- [38] E. J. Calvo, N. Mozhzhukhina, *Electrochem. Commun.* **2013**, *31*, 56–58.
- [39] T. K. Zakharchenko, A. Y. Kozmenkova, D. M. Itkis, E. A. Goodilin, *Beilstein J. Nanotechnol.* **2013**, *4*, 758–762.
- [40] R. Black, S. H. Oh, T. Yim, J. Lee, B. Adams, L. F. Nazar, *J. Am. Chem. Soc.* **2012**, *134*, 2902–2905.
- [41] B. D. Adams, R. Black, Z. Williams, R. Fernandes, M. Cuisinier, E. J. Berg, P. Novak, G. K. Murphy, L. F. Nazar, *Adv. Energy Mater.* **2014**, DOI: 10.1002/aenm.201400867.
- [42] M. Okoshi, Y. Yamada, A. Yamada, H. Nakai, *J. Electrochem. Soc.* **2013**, *160*, A2160–A2165.
- [43] M. J. Ziegler, J. D. Madura, *J. Solution Chem.* **2011**, *40*, 1383–1398.
- [44] S. Lau, L. A. Archer, *Nano Lett.* **2015**, DOI: 10.1021/acs.nanolett.5b02149.
- [45] M. R. Mitchell, B. M. Gallant, C. V. Thompson, Y. Shao-Horn, *Energy Environ. Sci.* **2011**, *4*, 2952.
- [46] N. B. Aetukuri, B. D. McCloskey, J. M. García, L. E. Krupp, V. Viswanathan, A. C. Luntz, *Nat. Chem.* **2015**, *7*, 50–56.
- [47] D. G. Kwabi, T. P. Batcho, C. V. Amanchukwu, N. Ortiz-Vitoriano, P. Hammond, C. V. Thompson, Y. Shao-Horn, *J. Phys. Chem. Lett.* **2014**, *5*, 2850–2856.
- [48] D. Sharon, M. Afri, M. Noked, A. Garsuch, A. A. Frimer, D. Aurbach, *J. Phys. Chem. Lett.* **2013**, *4*, 3115–3119.
- [49] N. Mozhzhukhina, L. P. Méndez De Leo, E. J. Calvo, *J. Phys. Chem. C* **2013**, *117*, 18375–18380.
- [50] A. Khetan, A. Luntz, V. Viswanathan, *J. Phys. Chem. Lett.* **2015**, *6*, 1254–1259.
- [51] K. Ueno, R. Tatara, S. Tsuzuki, S. Saito, H. Doi, K. Yoshida, T. Mandai, M. Matsugami, Y. Umeyayashi, K. Dokko et al., *Phys. Chem. Chem. Phys.* **2015**, *17*, 8248–8257.
- [52] K. Ueno, K. Yoshida, M. Tsuchiya, N. Tachikawa, K. Dokko, M. Watanabe, *J. Phys. Chem. B* **2012**, *116*, 11323–11331.
- [53] K. Fujii, H. Hamano, H. Doi, X. Song, S. Tsuzuki, K. Hayamizu, S. Seki, Y. Kameda, K. Dokko, M. Watanabe et al., *J. Phys. Chem. C* **2013**, *117*, 19314–19324.

Received: October 1, 2015





Revised: November 12, 2015

Published online: ■■■■■, ■■■■■

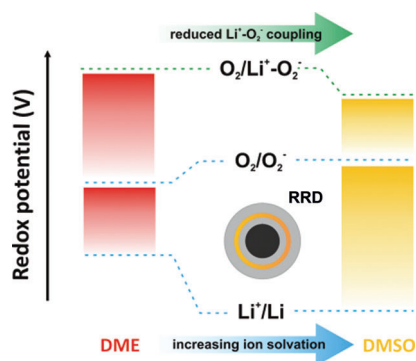
Communications



Oxygen Electrochemistry

D. G. Kwabi, V. S. Bryantsev, T. P. Batcho,
D. M. Itkis, C. V. Thompson,
Y. Shao-Horn*    

Experimental and Computational
Analysis of the Solvent-Dependent $O_2/$
 $Li^+-O_2^-$ Redox Couple: Standard
Potentials, Coupling Strength, and
Implications for Lithium–Oxygen
Batteries



The free-energy landscape of reactions involved in the Li oxygen reduction reaction (ORR) were obtained by rotating ring disk (RRD) measurements and calculations. Differences in redox potentials of O_2/O_2^- and $O_2/Li^+-O_2^-$ couples vs. Li^+/Li in dimethoxyethane (DME) and dimethylsulfoxide (DMSO) reflect the influence of increasing solvation on the free energy of O_2^- formation vs. Li^+/Li and $Li^+-O_2^-$ coupling.